ASTRONOMY & ASTROPHYSICS
SUPPLEMENT SERIES

Astron. Astrophys. Suppl. Ser. **104,** 365-376 (1994)

Evolutionary sequences of stellar models with new radiative opacities. III. Z=0.0004 and Z=0.05*

F. Fagotto[1], A. Bressan[2], G. Bertelli[1,3] and C. Chiosi[1]

[1] Department of Astronomy, Vicolo Osservatorio 5, 35122 Padua, Italy
[2] Astronomical Observatory, Vicolo Osservatorio 5, 35122 Padua, Italy
[3] Fellow of the National Council of Research CNR-GNA

Received June 17; accepted September 20, 1993

Abstract. — We present detailed tabulations of two large grids of stellar models with the extreme initial chemical composition [Z=0.0004, Y=0.230], and [Z=0.050, Y=0.352]. The models are computed with the most recent radiative opacities (OPAL) by Iglesias et al. (1992) and with the inclusion of overshoot from convective cores and envelopes according to the formalism by Bressan et al. (1981) and Alongi et al. (1991), respectively, and the revision made by Bressan et al. (1993a). These calculations represent the continuation of the series initiated with the paper by Bressan et al. (1993a) for the grid with [Z=0.020, Y=0.280] (the reference solar like abundance). The tracks are calculated for a wide range of initial masses from 0.6 $M_{\odot}$ to 120 $M_{\odot}$ and extend from the ZAMS till very advanced evolutionary phases. Specifically, low and intermediate mass stars are followed to the beginning of the TP-AGB, while massive stars are followed till the core C-ignition. The models of low and intermediate mass stars are calculated at constant mass, whereas those of massive stars are followed in presence of mass loss by stellar winds incorporating a suitable dependence on the metallicity. The results of all the models are given in extensive tables which summarize also the lifetimes of the various phases and the variations of surface abundances by dredge-up phenomena and mass loss by stellar wind. The salient features brought by the different metallicity and helium content are briefly outlined, with particular attention to the anomalous behaviour of the low mass, high metallicity stars in core He-burning and later phases. Such grids of evolutionary tracks are well indicated for studies of population synthesis in virtue of their large coverage of masses, evolutionary phases, and chemical composition. The high metallicity set is particularly suited to interpret the stellar content of bulges and elliptical galaxies.

Key words: stars: evolution — stars: interiors — stars: Hertzspung-Russell diagram — stars: abundances

1. Introduction

Stellar models are requested in order to study many astrophysical topics, e.g. color-magnitude diagrams (CMD) and luminosity functions (LF) of star clusters, stellar nucleosynthesis, spectro-photometric evolution of stellar populations, chemical evolution of galaxies, etc. To this aim a considerable effort has been devoted in achieving an evolutionary stellar data-base which has to be firstly complete in mass, chemical composition, and major evolutionary stages, and secondly homogeneous as well as up-dated in its physical ingredients.

This would avoid the introduction of intrinsic biases consequent to the application of inhomogeneous or incomplete grids that at least differ in many physical assumptions.

In particular, the recent achievements in the new radiative opacities by the Livermore Group (Iglesias et al. 1992, thereinafter OPAL) require the prompt calculation of stellar models incorporating these important results.

Up to now the only stellar models which satisfy the above request of homogeneity and physical accuracy and include the new radiative opacities are those presented in this paper, those by Bressan et al. (1993a) for the composition [Z=0.020, Y=0.280], those by Fagotto at al. (1993a, b) for the compositions [Z=0.001, Y=0.230], [Z=0.004, Y=0.240] and [Z=0.008, Y=0.250].

In fact the evolutionary tracks presented with OPAL by Stothers & Chin (1991) are too coarse in the mass coverage, whereas those by Schaller et al. (1992), Schaerer et al. (1993), and Charbonnel et al. (1993), for which a finer grid of stellar masses and accurate input physics were

Send offprint requests to: C. Chiosi

* Tables 1 to 4 are only available in electronic form: see the Editorial in A&AS 1994, Vol. 103, No. 1

adopted, are limited in the coverage of late evolutionary phases. Indeed they do not go beyond the tip of the red giant branch (RGB), thus hampering their use in the study of CMDs and LFs of old and intermediate age clusters.

In addition to the opacity, there is the long debated question on the type of mixing to be used for central and external convection, namely either the classical scheme or the overshoot scheme (see Chiosi et 1992a for a recent review of the subject) and the correlation with the opacity in use. In fact, some authors (Stothers & Chin 1991; Castellani et al. 1992) claimed that the changes in stellar lifetimes produced by OPAL would make unnecessary the presence of convective overshoot in order to reproduce the properties of CMDs and LFs of the Large Magellanic Cloud (LMC) clusters.

Besides the fact that this argument has been drawn from comparing OPAL models with old models based on the opacities of Cox & Stewart (1970a, b) between which there is a very large difference (Stothers & Chin 1991), it has also been proved by Bressan et al. (1993a) that the adoption of OPAL does not change the lifetime ratios between He- and H-burning phases both for classical and overshoot models. Indeed the above ratio for classical models is always too high to fully agree with the integrated LFs of intermediate age clusters of LMC, see for instance the recent studies by Vallenari et al. (1991, 1992, 1993). Therefore, the question of the type of mixing is still open.

In this paper, we present two large grids of stellar models with extreme initial chemical compositions, namely [Z=0.0004, Y=0.230], and [Z=0.05, Y=0.352] computed with the recent release of OPAL by Iglesias et al. (1992). The chemical parameters vary according to the law $\Delta Y/\Delta Z = 2.5$, a sort of lower limit to the commonly accepted rate of helium to metal enrichment (Pagel et al. 1992). The models are calculated with mild core and envelope overshoot according to the scheme summarized below.

2. Physical ingredients of the models

The physical input is the same as that used by Bressan et al. (1993a) according to the request of homogeneity as previously claimed. Therefore, we will limit ourselves to recall in major detail only two among the basic ingredients of the stellar computations that are worth putting into evidence, namely the opacity input and the mass-loss rates adopted.

In fact these two ingredients are very critical when applied to evolutionary tracks whose initial chemical composition is quite different from the solar one since both the opacity and the mass-loss rate are proportional to the metallicity.

As usual we endeavor to divide the evolutionary tracks into three groups in which the stars share similar properties. The subdivision is easily accomplished looking at the critical mass for which the ignition of the central fuel (helium or carbon) starts quietly depending on the level of core electron-degeneration.

Specifically low mass stars ($M \leq M_{\rm HeF}$) are those which ignite helium through a phase of violent burning episodes (Helium-Flash), intermediate mass stars are those which avoid core He-flash but develop an highly electron-degenerate carbon-oxygen core ($M_{\rm HeF} \leq M \leq M_{\rm up}$) and massive stars ($M \geq M_{\rm up}$) as those which are able to ignite carbon quietly.

Radiative opacity has suffered from constant refinement over the last few years by the Livermore group. We have adopted the recent tables by Iglesias et al. (1992 and references) which supersede the previous OPAL computations (Rogers & Iglesias 1992 and references) because of the inclusion of the spin-orbit interaction in the treatment of Fe atomic data and the adoption of the recent measurement of the solar photospheric Fe abundance by Grevesse (1991) and Hannaford et al. (1992).

We recall that the main feature of the OPAL is the presence of two enhancements with respect to the old opacity of Huebner et al. (1977, thereinafter LAOL), the most relevant (bump-like) being located near the temperature of a few hundred thousand degrees.

However the strength of this bump is critically related to the chemical composition, being higher at higher metal content, to the inclusion or not of the spin-orbit interactions, and to the mixture of the fractional abundances of metals adopted for the opacity calculation. For example the inclusion of the spin-orbit interactions enhances of 50% the quoted bump with the Anders & Grevesse (1989) Fe abundance and only of 25% with the Grevesse (1991) Fe abundance (Iglesias et al. 1992). Nowadays, the OPAL incorporating the spin-orbit interaction and the Grevesse (1991) mixture of abundances ought to be preferred. Finally, in these model calculations we include the contribution by the molecular opacity by means of the analytical relationships by Bessell et al. (1989, 1991).

Significant mass loss by stellar wind for low and intermediate mass stars comes only during the RGB and AGB phases. However, depending on the metallicity, a different approach has to be adopted. In the case of low metallicity models (Z=0.0004) both the RGB and AGB phase have a regular behaviour, which allows the inclusion of mass loss by means of the analytical method outlined long ago by Renzini (1977) and since then adopted in many studies (e.g. Bertelli et al. 1990; and Groenewegen & de Jong 1993). This means that going from the tip of the RGB to the zero age horizontal branch (ZAHB) the mass of the star can be simply scaled by removing a fraction of the envelope, whereas the evolution along the asymptotic giant branch (AGB) has to be followed numerically till the onset of the thermally pulsing regime of the He-burning shell (TP-AGB). Beyond this point the evolution can be followed analytically provided that the

relationship between the mass of the H-exhausted core, the total luminosity, and the rate of mass loss as a function of basic stellar parameters (e.g. luminosity, mass, and radius) are assigned. Therefore, the stellar models for this mass range and composition are calculated at constant mass.

The case of the stars with Z=0.05 is a more cumbersome affair because, whilst the RGB phase is regular, the evolution from ZAHB to the end of the AGB phase is more complicated, and depending on the star mass, there are sequences that fail to follow the regular scheme and therefore require the direct inclusion of mass loss in the models all the way down to the white dwarf stage (WD). The rate of mass loss adopted here is according to Reimers (1975) with $\eta = 0.35$.

On the contrary, for those sequences that follow the regular scheme, also in this case the effect of mass loss can be taken into account with the analytical method, and therefore they are calculated at constant mass.

Massive stars with initial mass $M \geq 12\ M_{\odot}$ are always evolved including the effect of mass loss by stellar wind from the ZAMS stage because their structure and evolution is entirely dominated by this phenomenon (Chiosi & Maeder 1986; Chiosi et al. 1992a, b). The empirical mass-loss rates are the same as in Bressan et al. (1993a), which are based upon observational data for supergiants, luminous blue variables (LBV), and Wolf Rayet (WR) stars. Precisely, they are derived from de Jager et al. (1988) for all evolutionary stages from the main sequence up to the so-called de Jager limit in the Hertzsprung Russell Diagram (HRD). Critical is the dependence of the rates on metallicity. As suggested by Kudritzki et al. (1989) this dependence is assumed to be

$$\dot{M}_Z = (Z/Z_{\odot})^{0.5} \times \dot{M}_{Z\odot}. \quad (1)$$

Beyond the De Jager limit, the mass-loss rate is increased to $10^{-3}\ M_{\odot}\ \mathrm{yr}^{-1}$ as suggested by the observational data for the LBV. The WR stages are supposed to begin when the surface fractionary abundance of hydrogen falls below the value 0.3 and the effective temperature is high enough. During these phases the mass-loss rate is derived according to the Langer (1989) prescription.

No correction to the effective temperature of the models is applied to account for the optical thickness of the stellar material in the wind. This correction does not affect the internal structure of the models and can be easily taken into account analytically (e.g. Bertelli et al. 1984; Schaller et al. 1992).

Finally, as already mentioned the models are calculated evaluating the extension of the convective regions (wherever necessary) by means of the overshoot scheme of mixing according to the prescriptions given by Bressan et al. (1981), Bertelli et al. (1985), Alongi et al. (1991, 1993), and Bressan et al. (1993a). The efficiency of this process has been preliminary calibrated on observational data for LMC clusters and Galactic old open clusters (see the discussion of this topic by Chiosi et al. 1992a). Current estimates indicate a mild efficiency of core overshoot ($\Lambda_c \leq 0.5$) and envelope overshoot (Λ_e=0.7). The physical motivations for the occurrence of the phenomenon of convective overshoot and its efficiency have been recently discussed by Zahn (1991), Canuto & Mazzitelli (1991), and Cattaneo et al. (1991).

For the sake of clarity, we would like to point out that our formalism for core overshoot leads to evolutionary results that are in strict agreement with those obtained by the Geneva group (Schaller et al. 1992; Schaerer et al. 1993; Charbonnel et al. 1993), in spite of the different values adopted for the parameter Λ_c.

This is due to the different algorithm used to calculate the overshoot distance. Indeed, while in Bressan et al. (1981) this is evaluated assuming that convective elements can travel a mean free path *across* the Schwarzschild border, in the Geneva group the overshoot distance is taken as a fraction of the local pressure scale height *above* the Schwarzschild border. It follows that our $\Lambda_c = 0.5$ is equivalent to their $\Lambda_c = 0.2$. This can easily be checked by comparing models with the same mass, chemical composition, and evolutionary phase.

The mixing length parameter α = l/Hp in the outermost super-adiabatic convective region is the same of Bressan et al. (1993a) which is calibrated on the solar model (VandenBerg 1991) and set equal to 1.63.

3. Evolutionary results and content of the tables

In the following we make a short discussion on some global features of the HRDs, lifetimes, and lifetime ratios of the major evolutionary phases, and the variation of the surface abundance induced by dredge-up and mass loss.

For each grid we summarize the evolutionary results by dividing them into specific sections. Precisely the results of the evolutionary tracks in the mass range 0.5 $M_{\odot}$ to 120 $M_{\odot}$ are presented following the classification in low, intermediate and high mass stars.

In the following, the labels 'A' and 'B' in the numeration of the tables and figures refer to the Z=0.0004 and Z=0.05 grids of the stellar models, respectively.

We inform the reader that Tables 1A, 1B through Tables 4A, 4B are not printed in the text, but are made available at the Centre de Données de Strasbourg via anonymous FTP according to the instructions published in the editorial notice of Astronomy & Astrophysics. They can also be obtained from the authors on request.

The quantities contained in the series of Tables from 1A, 1B to 4A, 4B have the following meaning:

- AGE: age of models in years
- $L/L_{\odot}$: logarithm (base 10) of the total luminosity in solar units
- $T_{\rm eff}$: logarithm (base 10) of the effective temperature

- G: logarithm (base 10) of the surface gravity
- T_c: logarithm (base 10) of the central temperature
- ρ_c: logarithm (base 10) of the central density
- COMP: central abundance (by mass) of hydrogen or helium
- X_C: central abundance of ^{12}C
- X_O: central abundance of ^{16}O
- Conv: fractionary mass of the convective core (inclusive of overshoot)
- Q_{disc}: fractionary mass of the first mesh point where the chemical composition differs from the surface value
- L_H: logarithm (base 10) of the hydrogen luminosity in solar units
- $Q1_H$: fractionary mass of the inner border of the hydrogen rich region
- $Q2_H$: fractionary mass of the outer border of the H-burning region. The boundary is taken where the nuclear energy generation rate becomes greater than a suitable value
- L_{He}: logarithm (base 10) of the helium luminosity in solar units
- $Q1_{He}$: fractionary mass of the inner border of the He-burning region (when greater than zero He-burning is in a shell). The boundary is taken where the nuclear energy generation rate becomes greater than a suitable value
- $Q2_{He}$: fractionary mass of the upper border of the He-burning region. The boundary is taken as above
- L_C: logarithm (base 10) of the carbon luminosity in solar units
- L_ν: logarithm (base 10) of the neutrinos luminosity (absolute value) in solar units
- Q_{Tmax}: fractionary mass of the point where the temperature attains the maximum value
- M_{dot}: logarithm (base 10) of the absolute value of the mass-loss rate in solar masses per year
- X_{sur}: surface abundance (by mass) of ^1H
- Y_{sur}: surface abundance (by mass) of ^4He
- XC_{sur}: surface abundance (by mass) of ^{12}C
- XN_{sur}: surface abundance (by mass) of ^{14}N
- XO_{sur}: surface abundance (by mass) of ^{16}O

The layout of Tables 4A, 4B is slightly different, because when the stellar winds are important, we also display the current mass of the star and the surface abundances (by mass) as indicated in the table headings. Tables 1A, 1B and 2A, 2B refer to the low mass range (stars undergoing core He-flash), and contain the data from the ZAMS to the tip of the RGB, and from the ZAHB to either the start of the TP-AGB phase (models with Z=0.0004) or the final WD cooling sequence (models with Z=0.05), respectively. Figures 1A, 1B, 2A, 2B show the corresponding HRDs of the evolutionary tracks. For the sake of clarity, Fig. 2B has been split in panel

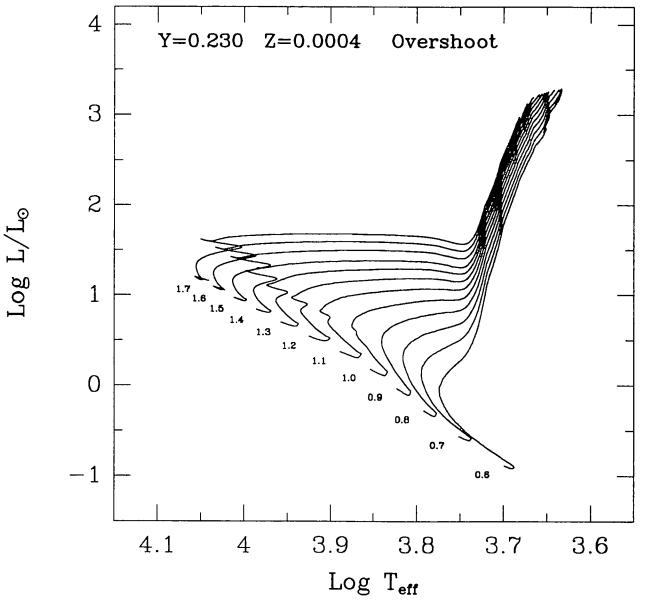

Fig. 1A. Theoretical HRD for the low mass stars with composition [Y=0.230, Z=0.0004]. Each evolutionary track goes from the ZAMS to the tip of the RGB. Models, in which during the core H-burning phase a convective core can develop, are calculated with mild overshoot. The parameter Λ_c is 0.25 in the mass range 1.0 $M_\odot \leq M \leq$ 1.4 $M_\odot$ and 0.5 above it. Overshoot at the bottom of the convective envelope along the Hayashi line is calculated with Λ_e = 0.7. The initial mass in solar unit is indicated along each curve

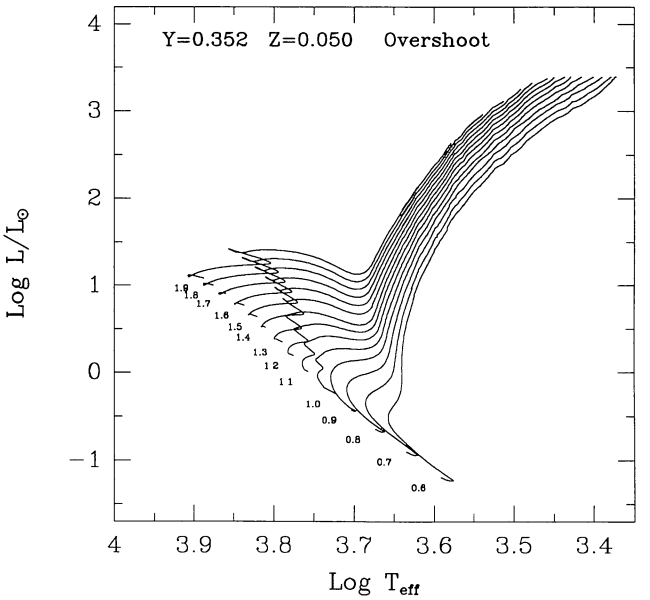

Fig. 1B. The same as the Fig. 1A for the composition [Y=0.352, Z=0.050]

(a) showing the core He-burning and later phases for a few models (with Z=0.05) with ZAHB mass in the range

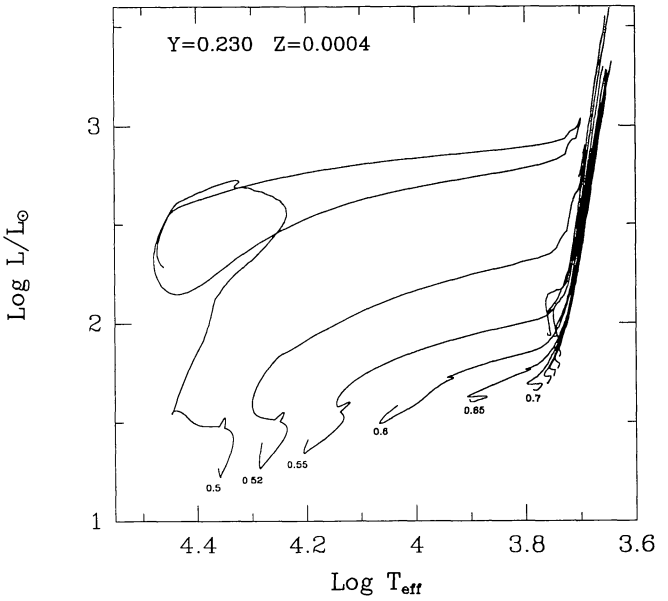

Fig. 2A. Theoretical HRD for low mass stars during the core He-burning phase. The chemical composition is [Y=0.230, Z=0.0004]. This models are calculated with the overshoot scheme. The mass of the stars in solar units is indicated along each evolutionary track. The models go from the ZAHB to the beginning of the TP-AGB phase

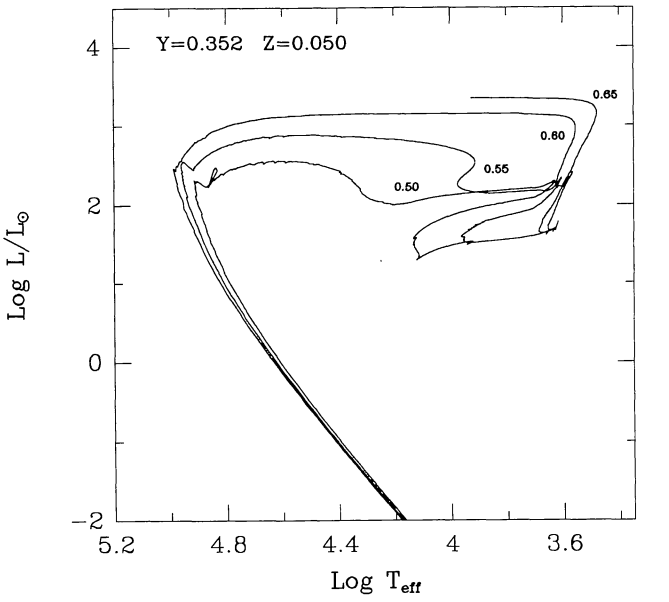

Fig. 2B. (Panel a) The same as the Fig. 2A for some low mass stars with composition [Y=0.352, Z=0.050]. Note that they evolve from the E-AGB toward higher temperature and, after a thermal instability, follow the WD cooling sequences

0.50 – 0.65 $M_\odot$, and panel (b) displaying the same but for ZAHB masses in the range 0.70 – 1.9 $M_\odot$.

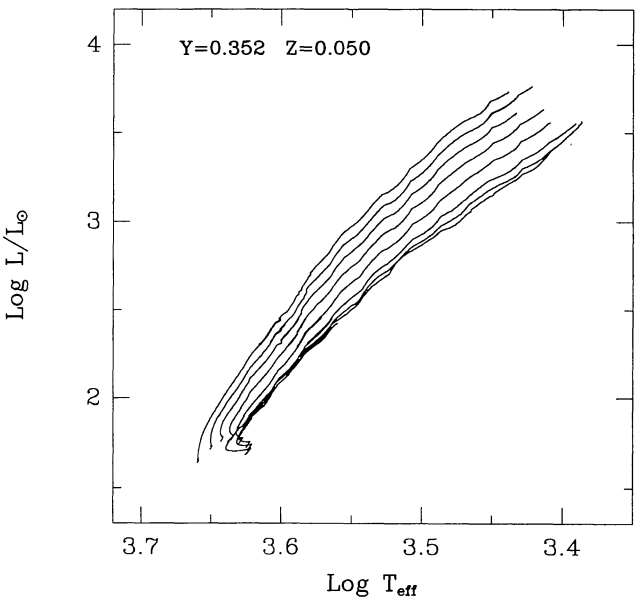

Fig. 2B. (Panel b) The same as the Fig. 2B (panel a) for the other low mass stars with composition [Y=0.352, Z=0.050]

Looking at the data of Tables 1A, 1B, 2A and 2B and Figs. 1A, 1B, 2A and 2B, several important differences emerge for the large-metallicity grid of low mass evolutionary tracks with respect to the low-metallicity one:

i) the transition mass from low to intermediate mass stars decreases from $M_{\rm HeF} = 1.9\ M_\odot$ to $M_{\rm HeF} = 1.7\ M_\odot$;

ii) the main sequence band is significantly larger;

iii) the temperature range covered by the SGBs is significantly narrower;

iv) the RGBs are more tilted toward lower temperatures.

The evolutionary path in HRDs of low mass stars during the core He-burning and later phases deserves a short discussion.

With low metallicity (Fig. 2A), the ZAHB is shifted to higher and higher temperatures at decreasing ZAHB mass. However for stars more massive than 0.52 $M_\odot$ following core He-exhaustion the models evolve toward the Hayashi line to start the AGB phase. On the contrary stars less massive than 0.52 $M_\odot$ settle on very hot temperature and proceed exhausting the central fuel growing their luminosity and maintaining their high temperature. The 0.5 $M_\odot$ with Z=0.0004 fails the classical AGB phase but moves toward higher luminosity until it turns on the thermal pulses which very rapidly displace the star from the hot to the cold part and viceversa of the HRD.

More anomalous is the behaviour of the low mass stars of high metallicity shown in Fig. 2B (panels a and b), which deserve a closer inspection.

We note how models with mass greater than about 0.65 $M_\odot$ as expected burn central helium at low effective

temperatures and evolve toward the start of the TP-AGB phase climbing along the Hayashi line. Stars of lower mass progressively shift to higher temperatures the location of the core He-burning phase at decreasing mass, and following core He-exhaustion tend to evolve toward the Hayashi line. However at different peculiar stages each star departs from the AGB before attaining the thermal pulses regime and crosses the HRD at high luminosity toward the planetary nebula stages. Finally, after a last thermal instability the stars approach and proceed along their white dwarf cooling curves.

It is evident from the present results and previous similar studies (Castellani et al. 1992, Horch et al. 1992) that for any given composition and efficiency of mass loss there is a critical ZAHB mass below which stars do not necessarily evolve along the AGB till to reach high luminosity before dramatically losing their envelope to ignite the planetary nebula phase, but follow the morphology as described above. This is ultimately related to the amount of mass in the envelope left over by mass loss during the RGB phase and the rate at which the H-exhausted core grows under the action of the H-burning shell during the core He-burning phase.

With the classical efficiency of mass loss during the RGB phase and compositions assigned to globular clusters (e.g. Y=0.230 and $Z << Z_{\odot}$), this limit mass is well below the typical ZAHB mass and therefore totally irrelevant to the analysis of the CMDs of globular clusters. As either Y or Z or both increase, the departure from the classical scheme occurs at progressively higher values of the ZAHB mass.

Limiting the discussion to the paradigmatic case of the interpretation of the CMD of a globular cluster, which requires a certain turn-off mass, HB mass, and age in addition to metallicity, several possibilities exist.

If the metallicity is kept constant and the helium abundance is supposed to increase with respect to the classical value (Y=0.230), the H-burning lifetime of a star of mass M decreases, whereas the luminosity increases. At given turn-off luminosity, the two effects lead to a smaller turn-off mass. As a consequence, the ZAHB mass is smaller and the above transition is facilitated. However, an increase in Y without a corresponding increase in metallicity is not likely on the basis of current understanding of stellar nucleosynthesis.

Conversely, keeping fixed Y and increasing Z, the most common assumption for the chemical parameters of globular clusters, there are two effects acting in the same sense. On one hand the increased metallicity can perhaps imply a stronger efficiency of mass loss during the RGB phase, which would yield lower ZAHB masses. A direct dependence of the RGB mass-loss rate on the metallicity is however not yet sustained by strong observational evidences (see Chiosi et al. 1992a for a recent review). On the other hand, the increased metallicity surely implies a stronger efficiency of the H-burning shell (processing hydrogen via the CNO cycle), which means a faster increase in the H-exhausted core and hence decrease in the envelope mass. When this falls below a certain limit, the models fail to follow the classical scheme. Also in this case the transition is expected to occur at higher ZAHB masses. However, this would require unusual high metallicities, which are not typical of globular clusters.

Finally, there is the case of both helium and metallicity increasing at a certain rate $\Delta Y/\Delta Z$.

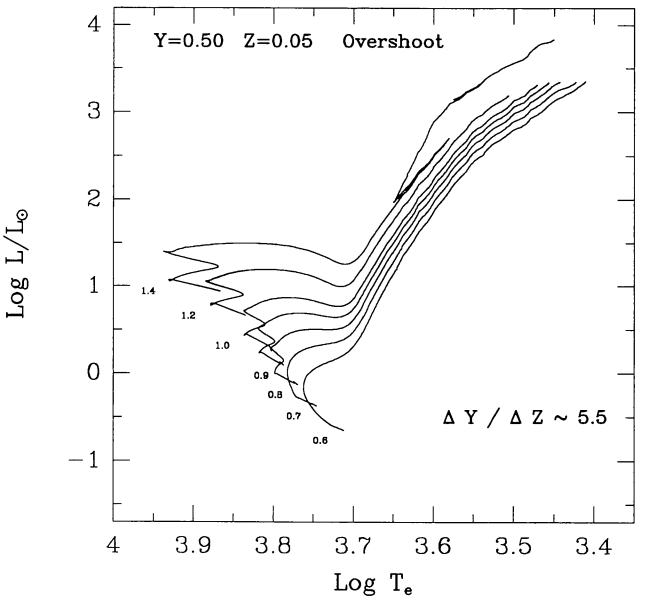

Fig. 3. Theoretical HRD for the low mass stars with composition [Y=0.50, Z=0.05]. Each evolutionary track goes from the ZAMS to the tip of the RGB. It has been reported also the 1.4 $M_{\odot}$ which ignite central He quiescently setting the critical mass $M_{\rm HeF}$ to a value significantly lower than the Y=0.352 case. Models, in which during the core H-burning phase a convective core can develop, are calculated with mild overshoot. The initial mass in solar unit is indicated along each curve

The present models are for $R \sim 2.5$ similarly to what assumed by Bressan et al. (1993a). This choice constitutes a lower limit to the values suggested by Pagel et al. (1992). In order to illustrate the effect of different choices for R we have computed a few tracks with Z=0.05 and $R \sim 5.5$. The evolution of these stars up to the tip of the RGB is shown in Fig. 3, whereas in Fig. 4 are displayed the corresponding core H-burning lifetimes. These tracks appear more luminous and hotter, a fact which coupled with the minor fuel available, makes very short their H-burning lifetimes for a given mass with respect to the corresponding less He-rich ones. Although the HB and later phases of these models were not calculated, their evolution in the HRD is easy to foresee. The data of Fig. 4 show that for ages of about 10 10^9 the turn-off mass is as low as 0.6 $M_{\odot}$. Allowing for a certain amount of mass

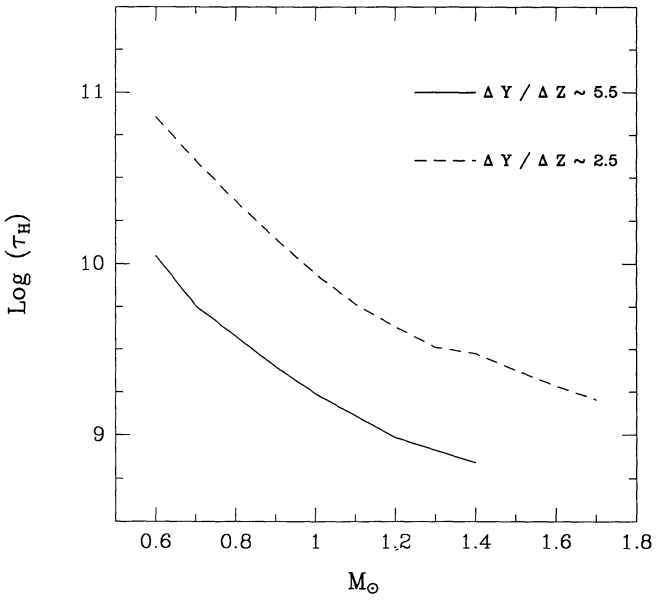

Fig. 4. Logarithm (base 10) of the H-burning lifetimes for the Z=0.05 grids of low mass evolutionary tracks for two choices of Helium enrichment parameter R versus initial mass of the star in solar units. Note the large decrement in lifetimes as R gets higher growing the possibility of having evolved very low mass stars which behave as strong UV emitters of elliptical galaxies (see text)

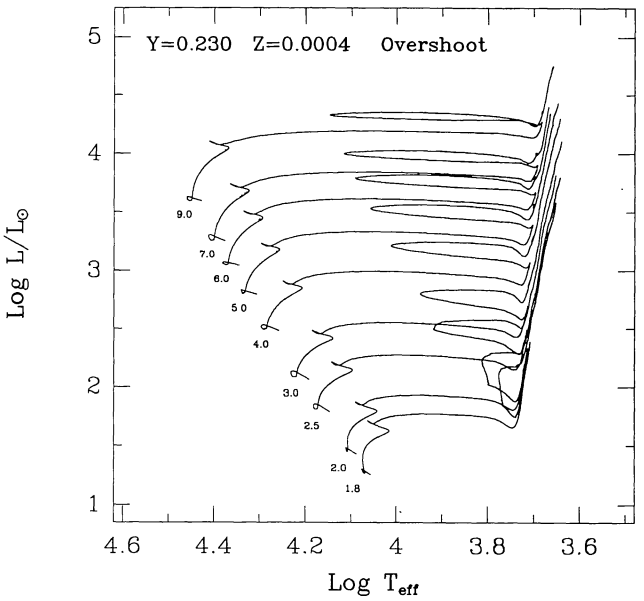

Fig. 5A. Theoretical HRD for intermediate mass and massive stars of lower mass with composition [Y=0.230, Z=0.0004]. Each evolutionary track goes from the ZAMS to either the start of the TP-AGB phase ($M \leq M_{up}$) or the stage of core C-ignition ($M \geq M_{up}$). These models are calculated with core and envelope overshoot ($\Lambda_c = 0.5$ and $\Lambda_e = 0.7$, respectively). The massive stars in the range $M_{up} \leq M \leq 9\ M_\odot$ are calculated at constant mass. The mass of the star in solar unit is indicated along each curve

loss during the RGB phase, the mass on the ZAHB can be easily as low as 0.5 $M_\odot$ or even lower. This automatically implies that a normal AGB phase for these stars is not possible, and that most likely they will behave as the 0.5 $M_\odot$ star of Fig. 2B (panel a), i.e. burning central helium at high effective temperatures and luminosities, and proceeding directly to the WD stage.

Tables 3A and 3B present the data for intermediate mass stars and those massive stars of lower mass in which the effect of mass loss by stellar wind can be neglected. The models go from the ZAMS to the latest evolutionary phase, i.e. TP-AGB for stars up to M_{up} and central C-ignition above. The values of M_{up} for both the metallicities fall between 5.0 $M_\odot$ and 6.0 $M_\odot$.

Figures 5A and 5B show the corresponding HRDs. The more impressive differences between the two cases is the different morphology of He-burning sequences. While the metal-poor tracks exhibit extended loops in the HRD, the metal-rich ones do not possess blue loops at all.

Tables 4A and 4B contain the models of massive stars in which the effect of mass loss all over their evolution is important. Each sequence goes from ZAMS to central C-ignition. The corresponding HRDs are shown in Figs. 6A and 6B. Relevant is the dependence of mass-loss rate on metallicity which strongly affects both the morphology of the HRD and the lifetimes of the various evolutionary

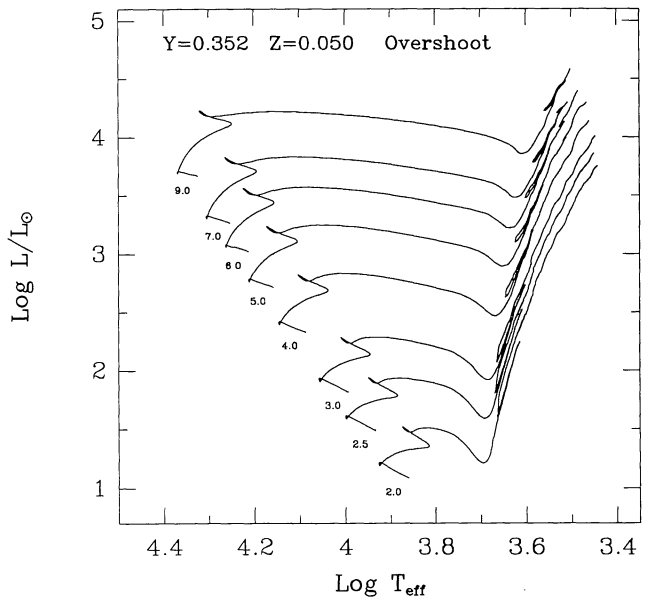

Fig. 5B. The same as the Fig. 5A for the intermediate mass and massive stars of lower mass with composition [Y=0.352, Z=0.050]

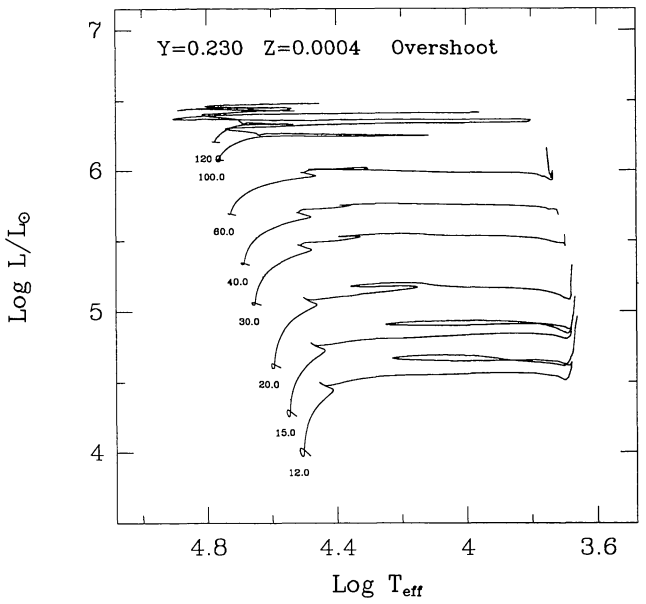

Fig. 6A. Theoretical HRD for massive stars with composition [Y=0.230, Z=0.0004] calculated with core and envelope overshoot, mass loss by stellar wind, and OPAL opacities. Each evolutionary track goes from the ZAMS to the stage of core C-ignition. The parameters for core and envelope overshoot are $\Lambda_c = 0.5$ and $\Lambda_e = 0.7$, respectively

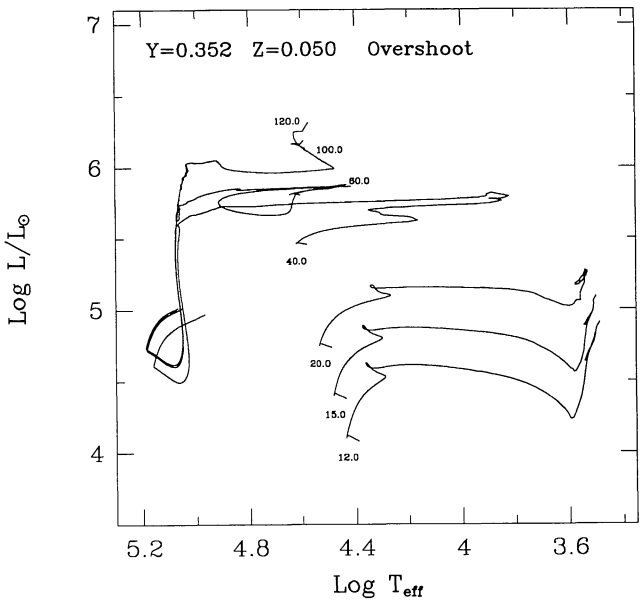

Fig. 6B. The same as in Fig. 6A for massive stars with composition [Y=0.352, Z=0.050]

phases. In particular the metal-poor models of any initial mass are found to never enter the Wolf-Rayet stages.

Tables 5A and 5B contain the lifetimes of the central H- and He-burning phases and early AGB (E-AGB) of all the models. The three lifetimes are indicated by $\tau_{\rm H}$, $\tau_{\rm He}$, and $\tau_{\rm E-AGB}$, respectively.

Table 5A. Lifetimes and lifetime ratios

OVERSHOOT			Z = 0.0004 Y=0.230	
$M/M_\odot$	τ_H	τ_{He}	τ_{He}/τ_H	τ_{EAGB}/τ_{He}
0.50		1.481E8		0.11
0.52		1.406E8		0.11
0.55		1.330E8		0.11
0.60	42.662E9	1.252E8	0.003	0.10
0.65		1.170E8		0.10
0.70	23.562E9	1.159E8	0.005	0.09
0.75		1.118E8		0.09
0.80	13.988E9	1.124E8	0.008	0.08
0.90	88.611E8	1.108E8	0.012	0.08
1.00	59.272E8			
1.10	41.254E8	1.010E8	0.024	0.09
1.20	29.779E8			
1.30	22.371E8	1.048E8	0.047	0.07
1.40	18.101E8			
1.50	15.556E8	1.064E8	0.068	0.06
1.60	12.764E8			
1.70	10.653E8	1.158E8	0.109	0.06
1.80	91.181E7	1.952E8	0.214	0.03
1.90	78.129E7	1.846E8	0.236	0.03
2.00	67.985E7	1.533E8	0.226	0.04
2.50	39.004E7	7.386E7	0.189	0.04
3.00	26.037E7	4.226E7	0.162	0.04
4.00	14.256E7	1.803E7	0.126	0.04
5.00	91.886E6	9.522E6	0.104	0.05
6.00	65.739E6	5.727E6	0.087	0.05
7.00	49.460E6	3.853E6	0.078	0.04
9.00	32.068E6	2.174E6	0.068	0.03
12.0	20.085E6	1.250E6	0.062	0.03
15.0	14.474E6	8.899E5	0.061	0.02
20.0	99.684E5	6.485E5	0.065	0.02
30.0	64.329E5	4.689E5	0.073	0.01
40.0	50.555E5	3.969E5	0.079	0.01
60.0	38.717E5	3.273E5	0.085	
100.0	30.508E5	2.681E5	0.088	
120.0	28.493E5	2.564E5	0.090	

Tables 6A and 6B summarize the changes in the surface abundances (by mass) induced by the first dredge-up (the pollution of the original surface composition by the products of H-burning) as function of the stellar mass. For the elements ^{1}H, ^{3}He, ^{4}He, ^{12}C, ^{13}C, ^{14}N, ^{15}N, ^{16}O, ^{17}O, and ^{18}O, this table displays both their initial abundance and their surface abundances after completion of the first dredge-up. The third column gives the fractionary mass ($Q_{\rm conv}$) of the layer reached by the external convection at its maximum penetration, while the last two columns show the ratios ^{12}C/^{13}C and $(^{14}{\rm N})/(^{14}{\rm N})_i$. This latter ratio is the enhancement factor of ^{14}N with respect to the initial value $(^{14}{\rm N})_i$.

Tables 7A and 7B indicate for each star the age at which the second dredge-up occurs (when the external convection reaches the deep He-rich layers between the inert carbon-oxygen core and the H-burning shell temporarily extinguished), the fractionary mass $Q_{\rm conv}$ of the layer reached by the external convection at its maximum

Table 5B. Lifetimes and lifetime ratios

	OVERSHOOT		Z = 0.050 Y=0.352	
$M/M_\odot$	τ_H	τ_{He}	τ_{He}/τ_H	τ_{EAGB}/τ_{He}
0.50		1.528E8		
0.55		1.305E8		
0.60	71.631E9	1.258E8	0.002	
0.65		1.257E8		
0.70	39.835E9	1.242E8	0.003	0.11
0.80	23.162E9	1.221E8	0.005	0.11
0.90	14.042E9	1.256E8	0.009	0.09
1.00	87.623E8			
1.10	58.330E8	1.161E8	0.020	0.11
1.20	42.755E8			
1.30	32.518E8	1.141E8	0.035	0.11
1.40	29.856E8			
1.50	23.822E8	1.244E8	0.052	0.09
1.60	19.203E8			
1.70	16.067E8	1.486E8	0.092	0.09
1.80	13.295E8			
1.90	11.360E8	2.041E8	0.180	0.07
2.00	97.731E7	2.578E8	0.264	0.05
2.50	50.556E7	1.523E8	0.301	0.06
3.00	30.275E7	7.851E7	0.259	0.07
4.00	14.121E7	2.249E7	0.159	0.09
5.00	80.342E6	8.784E6	0.109	0.11
6.00	52.038E6	4.649E6	0.089	0.11
7.00	36.800E6	2.918E6	0.079	0.08
9.00	21.760E6	1.576E6	0.072	0.05
12.0	12.964E6	9.325E5	0.072	0.04
15.0	92.458E5	7.013E5	0.076	0.02
20.0	64.503E5	5.350E5	0.083	0.02
40.0	36.720E5	6.637E5	0.181	
60.0	30.323E5	5.835E5	0.192	
100.0	25.220E5	5.921E5	0.235	
120.0	25.210E5	5.917E5	0.235	

penetration, and the surface abundances (by mass) of ^{1}H, ^{4}He, ^{12}C, ^{13}C, ^{14}N and ^{16}O.

In massive stars, the variation of the surface abundances in the course of evolution is not as simple as in the lower mass range, but it is complicated by the occurrence of mass loss and depends also on the efficiency of central mixing in the sense that the larger the convective core, the easier is the exhibition of nuclearly processed material at the surface. The variations in the surface abundances (by mass) of ^{1}H, ^{4}He, ^{12}C, ^{13}C, ^{14}N and ^{16}O expected for the assumed mixing (mild convective overshoot) and mass-loss rates are given in Tables 4A and 4B.

Finally, an important consequence straightly implied by the dependence of the internal structure and mass-loss rate on metallicity is that the nucleosynthetic predictions for the stellar yields are profoundly affected. Indeed, the yields for the early stages of galaxy evolution (low metallicity) can be significantly different with respect to those for late stages (high metallicity) (e.g. Maeder 1992). In any case, the yields are expected to vary with the chemical composition. This is an important drawback of current models of galactic chemical evolution, where yields for solar compositions are customarily adopted (see the discussion by Matteucci 1991).

4. Summary and conclusions

We have presented two new grids of evolutionary tracks with extremely low and high metallicity. They cover a wide range of evolutionary stages and masses and are suitable for population synthesis purposes. They complement those by Bressan et al. (1993a) to represent the whole stellar populations forming galaxies of any kind.

Results are given in tabular fashion and peculiar features of the models are briefly commented.

These grids of models belong to a wider data base of stellar models aimed at studying the spectro-photometric evolution of stellar populations of different complexity going from star clusters to galaxies. Part of this data base has already been published, the remaining will be published soon.

The following combinations of the chemical parameters are considered: [Y=0.230, Z=0.0004] (this paper), [Y=0.230, Z=0.001] (Fagotto et al.1993a), [Y=0.240, Z=0.004] and [Y=0.250, Z=0.008], (Fagotto et al. 1993b), [Y=0.280, Z=0.020] (Bressan et al 1993a), [Y=0.352, Z=0.050] (this paper), [Y=0.475, Z=0.10] (Fagotto et al. 1993c).

The sets with metallicities higher than solar (up to five times) are particularly useful to interpret the stellar content of bulges and elliptical galaxies.

It is known that high-metallicity stars populate the bulge of our Galaxy (Ortolani et al. 1992, 1993) but it is also believed to constitute an important stellar population of elliptical galaxies.

With the aid of the evolutionary models of the above grids and a new model of population synthesis, Bressan et al. (1993b) have studied the spectro-photometric evolution of elliptical galaxies with particular attention to the problem of the UV-excess and its correlation with the Mg_2 index, and hence metallicity (Burstein et al. 1988). Confirming and extending previous studies of the subject (Brocato et al. 1990; Castellani et al. 1992; Horch et al. 1992; Greggio & Renzini 1990), Bressan et al. (1993b) identify the main contributors to the UV-excess in the fraction of old stars with high metallicity and helium content during the hot HB and AGB manqué phases according to the classification proposed by Greggio & Renzini (1990).

This interpretation of the UV-excess is particularly robust and it provides the right correlation with the metallicity. Furthermore it imposes certain constraints on the helium to heavy element enrichment ratio $R = \Delta Y/\Delta Z$, and the rate of mass loss in the RGB and AGB phases.

Acknowledgements. This work has been financially supported by the Italian Ministry of University, Scientific Research and Technology (MURST) and the Italian Space Agency (ASI).

References

Alongi M., Bertelli G., Bressan A., Chiosi C. 1991, A&A 244, 95

Alongi M., Bertelli G., Bressan A. et al. 1993, A&AS 97, 851

Anders E., Grevesse N. 1989, Geochim. Cosmochim. Acta 53, 197

Bertelli G., Betto R., Bressan et al. 1990, A&AS 85, 845

Bertelli G., Bressan A., Chiosi C. 1984, A&A 130, 279

Bertelli G., Bressan A., Chiosi C. 1985, A&A 150, 33

Bessell M.S., Brett J.M., Scholz M., Wood P.R. 1989, A&AS 77, 1

Bessell M.S., Brett J.M., Scholz M., Wood P.R. 1991, A&AS Erratum, 621

Bressan A., Chiosi C., Fagotto F. 1993b, ApJS, submitted

Bressan A., Fagotto F., Bertelli G., Chiosi C. 1993a, A&AS 100, 647

Bressan A., Bertelli G., Chiosi C. 1981, A&A 102, 25

Brocato E., Matteucci F., Mazzitelli I., Tornambe' A. 1990, ApJ 349, 458

Burstein D., Bertola F., Buson L., Faber S.M., Lauer T.R. 1988, ApJ 328, 440

Canuto V, Mazzitelli I. 1991, ApJ 370, 295

Castellani V., Chieffi A., Straniero O. 1992, ApJS 78, 517

Cattaneo F., Brummel N.H., Toomre J., Lalagoli A., Hulburt N. E. 1991, ApJ 370, 282

Charbonnel C., Meynet G., Maeder A., Schaller G., Schaerer D. 1993, A&AS 101, 415

Chiosi C., Bertelli G., Bressan A. 1992a, ARA&A 30, 305

Chiosi C., Bertelli G., Bressan A. 1992b, in Instabilities in Evolved Super and Hypergiants, eds. C. de Jager & H. Nieuwenhuijzen (Amsterdam: North Holland Publ.) p. 145

Chiosi C., Maeder A. 1986, ARA&A 24, 239

Cox A.N., Stewart J.N. 1970a, ApJS 19, 243

Cox A.N., Stewart J.N. 1970b, ApJS 19, 261

de Jager C., Nieuwenhuijzen H., van der Hucht K.A. 1988, A&AS 72, 259

Fagotto F., Bressan A., Bertelli G., Chiosi C. 1993a, A&AS, to be submitted

Fagotto F., Bressan A., Bertelli G., Chiosi C. 1993b, A&AS, in press

Fagotto F., Bressan A., Bertelli G., Chiosi C. 1993c, A&AS, submitted

Greggio L., Renzini A. 1990, ApJ 364, 35

Grevesse N. 1991, A&A 242, 488

Groenewegen M.A.T., de Jong T. 1993, A&A, 267, 410

Hannaford P., Lowe R.M., Grevesse M., Noels A. 1992, A&A 259, 301

Horch E., Demarque P., Pinsonneault M. 1992, ApJ 388, L53

Huebner W.F., Merts A.L., Magee N.H., Argo M.F. 1977, Los Alamos Scientific Laboratory Report LA-6760-M

Iglesias C.A., Rogers F.J., Wilson B.G. 1992, ApJ 397, 717

Kudritzki R.P., Pauldrach A., Puls J., Abbot D.C. 1989, A&A 219, 205

Langer N. 1989, A&A 210, 93

Maeder A. 1992, A&A 264, 105

Matteucci F. 1991, in "Frontiers of Stellar Evolution", ed. D.L. Lambert, ASP Conference Ser. Vol 20, p. 539

Ortolani S., Bica E., Barbuy B. 1992, A&AS 92, 441

Ortolani S., Bica E., Barbuy B. 1993, A&A 267, 66

Pagel B.E.J., Simonson E.A., Terlevich R.J., Edmunds M.G. 1992, MNRAS 255, 325

Reimers D. 1975, Mem. Soc. R. Sci. Liege, ser. 6, Vol. 8, p. 369

Renzini A. 1977, in Advanced Stages of Stellar Evolution, eds. P. Bouvier & A. Maeder (Geneva Observatory) p. 151

Rogers F.J., Iglesias C.A. 1992, ApJS 79, 507

Schaerer D., Meynet G., Maeder A., Schaller G. 1993, A&AS 98, 523

Schaller G., Schaerer D., Meynet G., Maeder A. 1992, A&AS 96, 269

Stothers R.B., Chin C.W. 1991, ApJ 381, L67

Vallenari A., Chiosi C., Bertelli G. et al. 1991, A&AS 87, 517

Vallenari A., Chiosi C., Bertelli G. et al. 1992, AJ 104, 1100

Vallenari A., Aparicio A., Fagotto F., Chiosi C. 1993, A&A, submitted

VandenBerg D.A. 1991, in "The Formation and Evolution of Star Clusters", ed. K. Janes, ASPCS Vol. 13, 183

Zahn J.-P. 1991, A&A 252, 179

Table 6A. Surface abundances after the 1st dredge-up Z =0.0004, Y =0.230 overshoot

			^{1}H	^{3}He	^{4}He	^{12}C	^{13}C	^{14}N	^{15}N	^{16}O	^{17}O	^{18}O	^{12}C/^{13}C	^{14}N/^{14}N$_i$
INITIAL VALUES			0.770E+00	0.881E-06	0.230E+00	0.989E-04	0.12E-05	0.248E-04	0.98E-07	0.211E-03	0.84E-07	0.48E-06	83.46	1.00
M/M$_\odot$	AGE	Q_{CONV}	^{1}H	^{3}He	^{4}He	^{12}C	^{13}C	^{14}N	^{15}N	^{16}O	^{17}O	^{18}O	^{12}C/^{13}C	^{14}N/^{14}N$_i$
0.60	0.453E+11	0.476	0.763E+00	0.294E-02	0.234E+00	0.99E-04	0.119E-05	0.248E-04	0.97E-07	0.211E-03	0.84E-07	0.48E-06	82.81	1.00
0.70	0.253E+11	0.416	0.759E+00	0.220E-02	0.239E+00	0.98E-04	0.155E-05	0.249E-04	0.92E-07	0.211E-03	0.84E-07	0.48E-06	63.40	1.00
0.80	0.152E+11	0.371	0.757E+00	0.170E-02	0.241E+00	0.96E-04	0.251E-05	0.263E-04	0.85E-07	0.211E-03	0.84E-07	0.48E-06	38.45	1.06
0.90	0.981E+10	0.337	0.756E+00	0.134E-02	0.242E+00	0.92E-04	0.278E-05	0.310E-04	0.80E-07	0.211E-03	0.84E-07	0.48E-06	33.12	1.25
1.00	0.667E+10	0.309	0.754E+00	0.109E-02	0.244E+00	0.88E-04	0.293E-05	0.359E-04	0.75E-07	0.211E-03	0.87E-07	0.46E-06	29.99	1.45
1.10	0.469E+10	0.286	0.754E+00	0.910E-03	0.245E+00	0.84E-04	0.301E-05	0.397E-04	0.71E-07	0.211E-03	0.96E-07	0.45E-06	28.07	1.60
1.20	0.344E+10	0.267	0.754E+00	0.768E-03	0.245E+00	0.82E-04	0.315E-05	0.428E-04	0.68E-07	0.211E-03	0.12E-06	0.44E-06	25.96	1.72
1.30	0.260E+10	0.250	0.754E+00	0.658E-03	0.245E+00	0.78E-04	0.320E-05	0.466E-04	0.64E-07	0.211E-03	0.17E-06	0.42E-06	24.54	1.88
1.40	0.204E+10	0.236	0.754E+00	0.579E-03	0.245E+00	0.76E-04	0.329E-05	0.492E-04	0.61E-07	0.211E-03	0.20E-06	0.42E-06	23.13	1.98
1.50	0.166E+10	0.228	0.754E+00	0.521E-03	0.245E+00	0.73E-04	0.332E-05	0.527E-04	0.58E-07	0.211E-03	0.29E-06	0.40E-06	22.00	2.12
1.60	0.134E+10	0.219	0.754E+00	0.462E-03	0.245E+00	0.71E-04	0.341E-05	0.556E-04	0.56E-07	0.211E-03	0.48E-06	0.39E-06	20.66	2.24
1.70	0.111E+10	0.211	0.754E+00	0.402E-03	0.246E+00	0.67E-04	0.330E-05	0.602E-04	0.52E-07	0.211E-03	0.86E-06	0.37E-06	20.21	2.43
1.80	0.948E+09	0.207	0.755E+00	0.362E-03	0.245E+00	0.66E-04	0.331E-05	0.622E-04	0.51E-07	0.209E-03	0.13E-05	0.37E-06	19.88	2.51
1.90	0.808E+09	0.204	0.755E+00	0.320E-03	0.244E+00	0.64E-04	0.324E-05	0.654E-04	0.50E-07	0.208E-03	0.15E-05	0.36E-06	19.64	2.64
2.00	0.700E+09	0.205	0.755E+00	0.277E-03	0.244E+00	0.60E-04	0.334E-05	0.712E-04	0.45E-07	0.206E-03	0.15E-05	0.35E-06	17.94	2.87
2.50	0.397E+09	0.250	0.763E+00	0.190E-03	0.236E+00	0.63E-04	0.363E-05	0.679E-04	0.46E-07	0.206E-03	0.13E-05	0.36E-06	17.37	2.74
3.00	0.264E+09	0.316	0.765E+00	0.117E-03	0.235E+00	0.67E-04	0.341E-05	0.621E-04	0.53E-07	0.207E-03	0.10E-05	0.38E-06	19.76	2.50
4.00	0.144E+09	0.421	0.769E+00	0.950E-04	0.231E+00	0.74E-04	0.386E-05	0.509E-04	0.55E-07	0.211E-03	0.14E-06	0.42E-06	19.17	2.05
5.00	0.919E+08	0.554	0.769E+00	0.624E-04	0.230E+00	0.76E-04	0.404E-05	0.485E-04	0.56E-07	0.211E-03	0.10E-06	0.43E-06	18.83	1.95
6.00	0.657E+08	0.522	0.769E+00	0.503E-04	0.230E+00	0.78E-04	0.443E-05	0.457E-04	0.55E-07	0.211E-03	0.93E-07	0.44E-06	17.64	1.84
7.00	0.495E+08	0.488	0.769E+00	0.380E-04	0.230E+00	0.76E-04	0.432E-05	0.481E-04	0.53E-07	0.211E-03	0.98E-07	0.43E-06	17.62	1.94
9.00	0.321E+08	0.452	0.769E+00	0.246E-04	0.230E+00	0.71E-04	0.420E-05	0.546E-04	0.48E-07	0.211E-03	0.13E-06	0.41E-06	16.83	2.20

Table 6B. Surface abundances after the 1st dredge-up Z =0.050, Y =0.352 overshoot

			^{1}H	^{3}He	^{4}He	^{12}C	^{13}C	^{14}N	^{15}N	^{16}O	^{17}O	^{18}O	^{12}C/^{13}C	^{14}N/^{14}N$_i$
INITIAL VALUES			0.598E+00	0.110E-03	0.352E+00	0.124E-01	0.148E-03	0.310E-02	0.12E-04	0.264E-01	0.10E-04	0.61E-04	83.73	1.00
M/M$_\odot$	AGE	Q_{CONV}	^{1}H	^{3}He	^{4}He	^{12}C	^{13}C	^{14}N	^{15}N	^{16}O	^{17}O	^{18}O	^{12}C/^{13}C	^{14}N/^{14}N$_i$
0.60	0.777E+11	0.336	0.583E+00	0.270E-02	0.365E+00	0.123E-01	0.201E-03	0.311E-02	0.11E-04	0.264E-01	0.10E-04	0.61E-04	61.15	1.00
0.70	0.443E+11	0.296	0.583E+00	0.201E-02	0.365E+00	0.121E-01	0.290E-03	0.322E-02	0.11E-04	0.264E-01	0.11E-04	0.60E-04	41.80	1.04
0.80	0.267E+11	0.265	0.582E+00	0.155E-02	0.366E+00	0.117E-01	0.341E-03	0.363E-02	0.10E-04	0.264E-01	0.11E-04	0.60E-04	34.43	1.17
0.90	0.170E+11	0.240	0.583E+00	0.123E-02	0.366E+00	0.114E-01	0.360E-03	0.403E-02	0.98E-05	0.264E-01	0.11E-04	0.59E-04	31.58	1.30
1.00	0.108E+11	0.221	0.584E+00	0.991E-03	0.364E+00	0.110E-01	0.385E-03	0.438E-02	0.93E-05	0.264E-01	0.11E-04	0.56E-04	28.72	1.41
1.10	0.743E+10	0.205	0.585E+00	0.812E-03	0.364E+00	0.107E-01	0.399E-03	0.481E-02	0.89E-05	0.264E-01	0.11E-04	0.57E-04	26.77	1.55
1.20	0.541E+10	0.190	0.587E+00	0.672E-03	0.362E+00	0.103E-01	0.414E-03	0.520E-02	0.85E-05	0.264E-01	0.12E-04	0.56E-04	24.95	1.68
1.30	0.401E+10	0.179	0.588E+00	0.565E-03	0.361E+00	0.100E-01	0.430E-03	0.551E-02	0.81E-05	0.264E-01	0.13E-04	0.46E-04	23.35	1.77
1.40	0.321E+10	0.173	0.589E+00	0.519E-03	0.360E+00	0.986E-02	0.434E-03	0.572E-02	0.79E-05	0.264E-01	0.13E-04	0.54E-04	22.71	1.84
1.50	0.253E+10	0.169	0.590E+00	0.448E-03	0.359E+00	0.962E-02	0.429E-03	0.600E-02	0.77E-05	0.264E-01	0.24E-04	0.53E-04	22.41	1.93
1.60	0.203E+10	0.166	0.590E+00	0.390E-03	0.359E+00	0.945E-02	0.431E-03	0.620E-02	0.75E-05	0.264E-01	0.59E-04	0.52E-04	21.95	2.00
1.70	0.168E+10	0.164	0.590E+00	0.343E-03	0.360E+00	0.937E-02	0.425E-03	0.632E-02	0.74E-05	0.263E-01	0.11E-03	0.52E-04	22.03	2.03
1.80	0.139E+10	0.162	0.589E+00	0.308E-03	0.360E+00	0.929E-02	0.426E-03	0.642E-02	0.73E-05	0.263E-01	0.15E-03	0.52E-04	21.79	2.07
1.90	0.118E+10	0.162	0.588E+00	0.278E-03	0.361E+00	0.922E-02	0.427E-03	0.652E-02	0.72E-05	0.262E-01	0.21E-03	0.51E-04	21.60	2.10
2.00	0.101E+10	0.161	0.587E+00	0.252E-03	0.362E+00	0.904E-02	0.413E-03	0.678E-02	0.72E-05	0.261E-01	0.27E-03	0.42E-04	21.87	2.18
2.50	0.518E+09	0.163	0.583E+00	0.174E-03	0.366E+00	0.903E-02	0.425E-03	0.689E-02	0.71E-05	0.258E-01	0.43E-03	0.50E-04	21.23	2.22
3.00	0.308E+09	0.171	0.582E+00	0.136E-03	0.367E+00	0.902E-02	0.428E-03	0.697E-02	0.70E-05	0.257E-01	0.47E-03	0.50E-04	21.08	2.25
4.00	0.143E+09	0.199	0.583E+00	0.102E-03	0.367E+00	0.927E-02	0.450E-03	0.677E-02	0.70E-05	0.256E-01	0.40E-03	0.51E-04	20.61	2.18
5.00	0.808E+08	0.231	0.584E+00	0.876E-04	0.366E+00	0.944E-02	0.471E-03	0.662E-02	0.70E-05	0.256E-01	0.34E-03	0.52E-04	20.04	2.13
6.00	0.522E+08	0.260	0.583E+00	0.801E-04	0.367E+00	0.950E-02	0.467E-03	0.664E-02	0.71E-05	0.255E-01	0.33E-03	0.52E-04	20.32	2.14
7.00	0.369E+08	0.288	0.583E+00	0.745E-04	0.367E+00	0.942E-02	0.478E-03	0.678E-02	0.68E-05	0.255E-01	0.32E-03	0.52E-04	19.70	2.18
9.00	0.218E+08	0.337	0.582E+00	0.701E-04	0.367E+00	0.951E-02	0.488E-03	0.676E-02	0.68E-05	0.253E-01	0.32E-03	0.52E-04	19.49	2.18

Table 7A. Z =0.0004, Y =0.230 overshoot, surface abundances after the 2nd dredge-up

$M/M_\odot$	AGE	Q_{CONV}	^1H	^4He	^{12}C	^{13}C	^{14}N	^{16}O
1.8	0.115E+10	0.327	0.754E+00	0.245E+00	0.637E-04	0.34E-05	0.646E-04	0.209E-03
1.9	0.999E+09	0.321	0.755E+00	0.245E+00	0.613E-04	0.33E-05	0.680E-04	0.208E-03
2.0	0.860E+09	0.308	0.755E+00	0.244E+00	0.599E-04	0.33E-05	0.716E-04	0.206E-03
2.5	0.475E+09	0.287	0.763E+00	0.236E+00	0.631E-04	0.36E-05	0.679E-04	0.206E-03
3.0	0.309E+09	0.281	0.764E+00	0.235E+00	0.674E-04	0.34E-05	0.621E-04	0.207E-03
4.0	0.163E+09	0.244	0.727E+00	0.272E+00	0.595E-04	0.32E-05	0.865E-04	0.190E-03
5.0	0.103E+09	0.209	0.690E+00	0.309E+00	0.532E-04	0.30E-05	0.106E-03	0.177E-03
6.0	0.724E+08	0.257	0.723E+00	0.277E+00	0.540E-04	0.32E-05	0.100E-03	0.182E-03
7.0	0.539E+08	0.305	0.756E+00	0.244E+00	0.562E-04	0.33E-05	0.912E-04	0.189E-03
9.0	0.345E+08	0.332	0.753E+00	0.246E+00	0.547E-04	0.33E-05	0.962E-04	0.185E-03

Table 7B. Z =0.050, Y =0.352 overshoot, surface abundances after the 2nd dredge-up

$M/M_\odot$	AGE	Q_{CONV}	^1H	^4He	^{12}C	^{13}C	^{14}N	^{16}O
3.00	0.391E+09	0.220	0.582E+00	0.367E+00	0.900E-02	0.43E-03	0.700E-02	0.257E-01
4.00	0.165E+09	0.230	0.583E+00	0.367E+00	0.927E-02	0.45E-03	0.677E-02	0.256E-01
5.00	0.896E+08	0.254	0.583E+00	0.366E+00	0.943E-02	0.47E-03	0.662E-02	0.256E-01
6.00	0.567E+08	0.280	0.583E+00	0.367E+00	0.950E-02	0.47E-03	0.663E-02	0.255E-01
7.00	0.397E+08	0.306	0.583E+00	0.367E+00	0.942E-02	0.48E-03	0.678E-02	0.255E-01
9.00	0.233E+08	0.351	0.582E+00	0.367E+00	0.951E-02	0.49E-03	0.676E-02	0.253E-01